Journal of Biomedical Optics

BiomedicalOptics.SPIEDigitalLibrary.org

Implementation of fluorescence confocal mosaicking microscopy by "early adopter" Mohs surgeons and dermatologists: recent progress

Manu Jain
Milind Rajadhyaksha
Kishwer Nehal

SPIE.

Manu Jain, Milind Rajadhyaksha, Kishwer Nehal, "Implementation of fluorescence confocal mosaicking microscopy by "early adopter" Mohs surgeons and dermatologists: recent progress," *J. Biomed. Opt.* **22**(2), 024002 (2017), doi: 10.1117/1.JBO.22.2.024002.

Journal of Biomedical Optics 22(2), 024002 (February 2017)

REVIEW

Implementation of fluorescence confocal mosaicking microscopy by "early adopter" Mohs surgeons and dermatologists: recent progress

Manu Jain,* Milind Rajadhyaksha, and Kishwer Nehal
Memorial Sloan Kettering Cancer Center, Dermatology Service, Department of Medicine, New York, United States

Abstract. Confocal mosaicking microscopy (CMM) enables rapid imaging of large areas of fresh tissue *ex vivo* without the processing that is necessary for conventional histology. When performed in fluorescence mode using acridine orange (nuclear specific dye), it enhances nuclei-to-dermis contrast that enables detection of all types of basal cell carcinomas (BCCs), including micronodular and thin strands of infiltrative types. So far, this technique has been mostly validated in research settings for the detection of residual BCC tumor margins with high sensitivity of 89% to 96% and specificity of 99% to 89%. Recently, CMM has advanced to implementation and testing in clinical settings by "early adopter" Mohs surgeons, as an adjunct to frozen section during Mohs surgery. We summarize the development of CMM guided imaging of *ex vivo* skin tissues from bench to bedside. We also present its current state of application in routine clinical workflow not only for the assessment of residual BCC margins in the Mohs surgical setting but also for some melanocytic lesions and other skin conditions in clinical dermatology settings. Last, we also discuss the potential limitations of this technology as well as future developments. As this technology advances further, it may serve as an adjunct to standard histology and enable rapid surgical pathology of skin cancers at the bedside.
[DOI: 10.1117/1.JBO.22.2.024002]

Keywords: confocal mosaicking microscopy; Mohs surgery; ex vivo; basal cell carcinoma; frozen section; fresh tissue; histopathology; acridine orange.

Paper 160756SSVR received Nov. 1, 2016; accepted for publication Jan. 20, 2017; published online Feb. 15, 2017.

1 Introduction

An estimated 5.4 million cases of nonmelanocytic skin cancers (NMSCs) are diagnosed annually in the U.S.[1] Basal cell carcinoma (BCC) is the most common form of NMSC,[2] accounting for more than 4 million cases per year followed by squamous cell carcinoma (SCC) that accounts for 1 million cases per year.[1,3] Mohs microscopic surgery (MMS) is a specialized technique for the treatment of NMSCs. On an average, one in four cases of skin cancer is treated with MMS.[4] With the rise in the incidence of NMSCs, Mohs surgery also increased by two times during 2001 to 2006.[5,6] Currently, an estimated 1.5 million surgeries are performed every year, with treatments costs of about $2 billion.[7]

Mohs surgery allows surgeons to obtain clear tumor margins while maximizing normal tissue preservation, making it the treatment of choice for recurrent BCCs and for BCCs on anatomically sensitive areas, such as the face.[8] Precise tumor clearance during Mohs surgery is achieved by excising thin layers sequentially and mapping residual skin cancer. In cases with subclinical tumor extension, multiple excisions may be needed to reach clear surgical margins. Frozen sections of each excision are prepared during surgery and evaluated for the presence and location of residual tumor to guide subsequent excision. However, preparation of frozen sections involves tissue processing (freezing, sectioning, and staining), making it a labor-intensive and time-consuming process (~20 to 40 min/excision).[9] Frozen sectioning may also introduce freezing artifacts that could hinder residual tumor margin assessment.[10] In addition to these limitations, the preparation of frozen sections requires a specialized laboratory set-up and a trained Mohs technician, raising the overall cost of the Mohs surgery and pathology procedure.[4]

To overcome the limitations of the frozen sectioning process and provide rapid histopathological evaluation of *ex vivo* fresh tissue, several optical imaging techniques are being explored, such as confocal mosaicking microscopy,[9,11–15] fluorescence polarization,[16] multiphoton laser scanning microscopy,[17] fluorescence lifetime imaging,[18] Raman spectroscopy,[19] integrated autofluorescence and Raman scattering microscopy,[20] optical coherence tomography (OCT),[21] full-field OCT,[22] coherent anti-Stokes Raman scattering microscopy,[23] multimodal spectral imaging,[24] and terahertz spectral imaging.[25,26] Confocal mosaicking microscopy (CMM) is currently the furthest advanced, being implemented and validated in Mohs surgical settings in real time.[27–31] In these settings, CMM is being integrated into the clinical workflow and has shown high sensitivity and specificity for detecting residual BCC tumors in fresh Mohs surgical excisions. In this article, we assess the progress of CMM-guided Mohs surgery from bench-top development in a laboratory to actual bedside implementation in Mohs surgical settings. We will also discuss the current limitations of CMM and opportunities for future advancement in this field.

2 Confocal Mosaicking Microscopy

CMM enables rapid imaging of large areas of fresh and thick *ex vivo* tissue at cellular resolution, similar to histopathology,

*Address all correspondence to: Manu Jain, E-mail: jainm@mskcc.org

but without the need for traditional freezing and sectioning.[9,11–15] Imaging can be performed with either reflectance or fluorescence contrast. Images can be acquired in reflectance mode, called reflectance confocal microscopy (RCM),[9,11,12,15] and in fluorescence mode, called fluorescence confocal microscopy (FCM),[13,14] with the use of contrast agents, which is ideal for the evaluation of *ex vivo* tissues. The use of contrast agents during RCM or FCM imaging is similar to the use of stains in histology: to increase the detectability of tumor by increasing the contrast between nuclei, cells, and the dermal collagen.[9,13,14] High-resolution images are acquired and stitched together to create mosaics that display large areas of tissue at the equivalent of 1× or 2× magnification, as necessary for pathology. Furthermore, zooming in these large mosaics with higher magnifications (4× to 30×) is feasible when necessary. This procedure closely mimics the reading of frozen sections by Mohs surgeons, which routinely starts with 2× magnification to examine the entire excision, followed by, when necessary, 4× and then 10× to more closely inspect suspicious or ambiguous areas.

Acquisition and stitching of images may be performed in several ways. The traditional approach is to acquire a two-dimensional raster-sequence of standard square-shaped images with aspect ratios of ∼1∶1 and stitch together into a mosaic.[9,11,12,15] With this approach, each image must be aligned, registered, and stitched along both its length and width to two neighboring images, and we must correct for illumination fall-off (vignetting) artifacts in two dimensions. The original bench-top development of this approach for Mohs surgery application[9,11,12,15] was subsequently engineered into a commercially available CMM [VivaScope^{R} 2000; Caliber Imaging and Diagnostics (formerly, Lucid, Inc.), Rochester, New York].

A relatively new approach is to acquire a one-dimensional sequence of rectangular-shaped long strip images with aspect ratio of ∼1∶25 or longer.[32] With this newer strip mosaicking approach, each image must be aligned, registered, and stitched only along its length to only one neighboring image, and we must correct for illumination fall-off artifacts in only one dimension. This approach requires 50% less time for aligning, registering, and stitching and also 50% less corrections for illumination fall-off artifacts. Thus, the strip mosaicking approach is faster relative to the earlier traditional approach. Further details on the actual implementation in CMM hardware, including the algorithms and custom-designed software for stitching images, will be found in our earlier papers, for both the traditional mosaicking approach[9,11,12,15] and the newer strip mosaicking approach.[32]

Fresh tissues from Mohs surgery are living and wet with irregular shapes, topography, sizes, and compliance and are, therefore, difficult to mount for microscopy. Imaging on large areas of such tissue, especially to acquire a contiguous sequence of images to create mosaics, requires accurate and repeatable mounting and control of the position, orientation, and flatness of the surface to be imaged. Tissue mounting and control may be accomplished in several ways and with specialized devices.[9,11,12,15,32] Each approach requires the ability to mount Mohs surgical excisions, gently and uniformly flatten the surface to be imaged against an optically transparent (usually, glass) window, and accurately tweak its position and orientation with tip, tilt, and sag control. The functionality of the device must mimic the manual procedure of Mohs histotechnicians and the operation of cryostats that are routinely used for preparing frozen pathology sections for Mohs surgery. Devices include mechanical tissue fixtures, tissue cassettes, and glass window "sandwiches," with the use of compliant materials, such as gels and bladders for tissue flattening. Further details on example devices and implementation will be found in our earlier papers.[9,11,12,15,32]

2.1 *Development of Confocal Mosaicking Microscopy Imaging Protocol in Laboratory Settings*

Rajadhyaksha et al.[9] described the use of 5% acetic acid and confocal cross-polarized microscopy to image thick skin excisions containing BCC and SCC obtained from Mohs surgery. Acetic acid was used as a contrast agent to "aceto-whiten" or brighten nuclei in reflectance mode.[9,11,12,15] However, the surrounding normal dermis also appears bright. Consequently, large and densely nucleated tumors, such as superficial and nodular BCCs (Fig. 1), were readily identified, whereas small and sparsely nucleated tumors, such as micronodular and thin strands or cords of infiltrative and sclerosing BCC tumors, were lost in the background (Fig. 2). Later studies that were conducted on larger sample sizes using RCM-acetic acid approach also reported similar limitations.[27]

Therefore, RCM-acetic acid methodology was, subsequently, replaced by FCM imaging again using specific nuclear contrast agents but in fluorescence, such as acridine orange, methylene blue, and toluidine blue;[13,14] methylene blue and toluidine blue primarily stain nucleic acid (DNA and RNA) and are frequently used as conventional histology stains.[13] Acridine orange interacts with the DNA and RNA of the nuclei, without staining collagen tissue.[14] Thus, when stained tissue is imaged in fluorescence mode, the nuclei appear bright with minimal to weak interfering signal from collagen, imparting good contrast for the detection of even small tumor nests or cords[13,14] (Fig. 3).

Of these contrast agents, acridine orange has been, to date, more widely tested in skin, both for optimal use and staining[14,33] and, subsequently, for use in Mohs surgery.[27–31] Gareau et al.[14] demonstrated the FCM with acridine orange (FCM-acridine orange) method to be able to detect both large (and densely nucleated) as well as small (and sparsely nucleated) residual BCC tumors in Mohs surgical margins. Bini et al.[33] determined the optimal staining approach, in terms of concentration and immersion time, for maximizing contrast and detectability. Fifty discarded and thawed Mohs skin excisions were stained with a variable concentration (0.3 to 1.0 mM) of acridine orange for various periods of time (5 to 120 s). A concentration of 0.6 mM and immersion for 20 s was discovered to be optimal for detection of both large and small tumors and was subsequently validated on 50 more discarded samples.[14]

A modified research breadboard version of a Vivascope 2000 was used for imaging in fluorescence mode, with illumination of 488 nm, a water immersion 30×, and 0.9 numerical aperture objective lens.[14] Specialized devices and methods were developed for mounting and flattening Mohs surgical skin excision.[12,14] This system provided optical sectioning up to ∼1 μm and high resolution images of ∼0.25 μm. Individual images were acquired and up to 36×36 images stitched and processed to create mosaics that displayed field-of-view (FoV) of up to 12 mm × 12 mm, which is equivalent to a 2× view in standard light microscopy [Figs. 4(a) and 4(b)].[14] Further zooms at high magnifications of 10× to 30× were feasible when necessary [Figs. 5(a) and 5(b)].[14] The procedure for creating

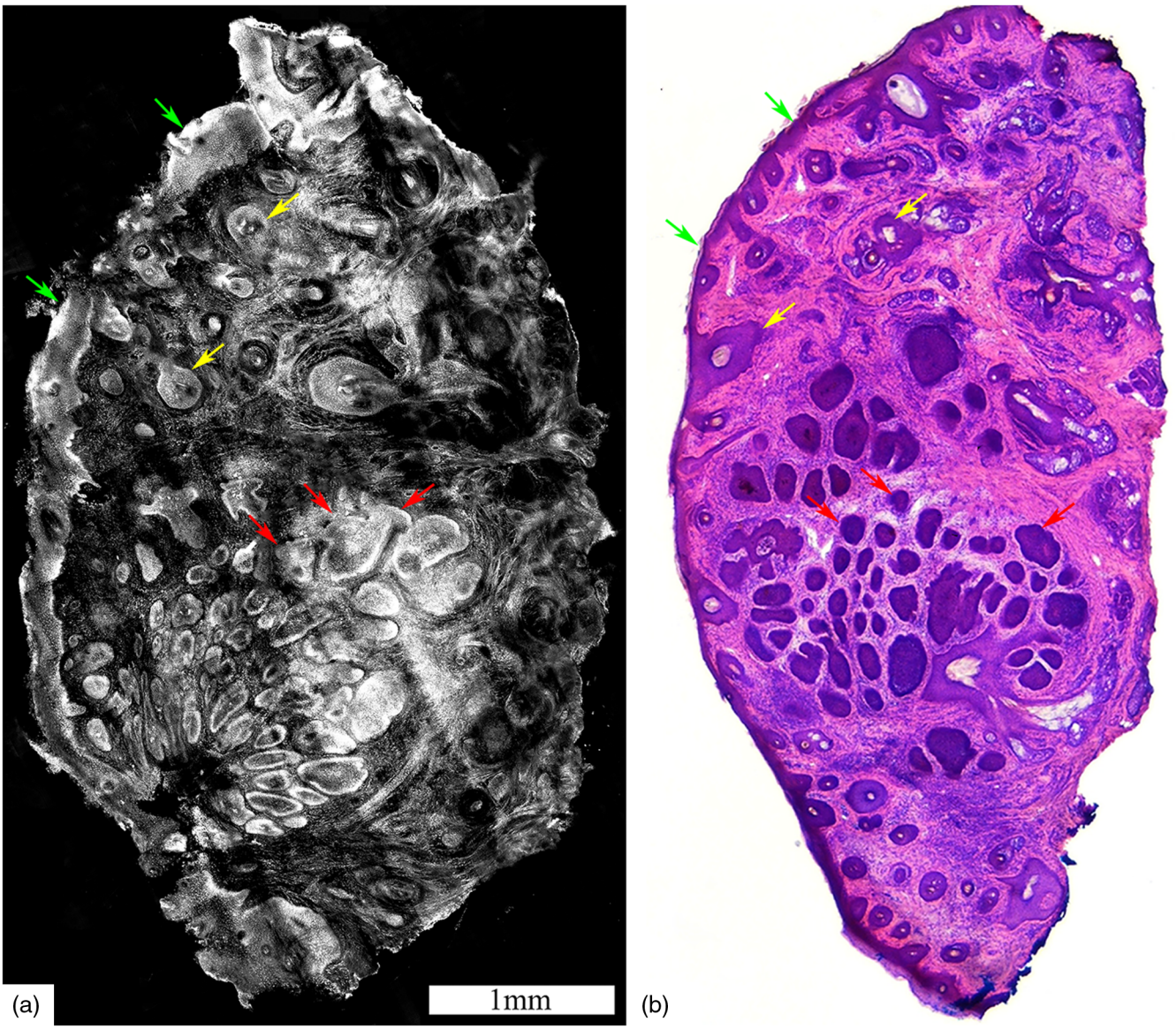

Fig. 1 Acetic acid stained reflectance confocal mosaic (a) shows nodular BCCs (red arrows) that can be readily identified at 2× magnification and compares well to (b) the corresponding H&E frozen histopathology. Nests of tumor (red arrows) within the dermis, the epidermal margin (green arrows) and hair follicles (yellow arrows) are seen. Scale bars: A = 1 mm. Figure reproduced with permission, courtesy of Wiley.[15]

a single mosaic required ~9 min. All subtypes of BCC (superficial, nodular, micronodular, infiltrative, and sclerosing) were imaged. Comparison of fluorescence mosaics to histology showed that this method detected both large and small tumors at low magnification [2×; Figs. 4(a) and 4(b)]. Although thin strands of infiltrative BCC could be readily identified in the collagenous background (in contrast to imaging with acetic acid) at low magnification (2×), it can sometimes be difficult to detect them in the background of bright nucleated structures, especially inflammatory cells, and required investigation at higher magnification (4× to 10×; Fig. 3). Similar challenge is also encountered on histology. Not only did Gareau et al.[14] demonstrate that acridine orange in fluorescence is a better contrast agent than acetic acid in reflectance for the detection of small and thin strands of tumors, but they also found that acridine orange does not interfere with subsequent histopathological evaluation. Thus, this study proved the feasibility of using FCM-acridine orange for the rapid detection of both small and large BCC tumors.

To validate their results, the same group later performed a semiquantitative preclinical study using the same experimental set-up on discarded BCC Mohs excisions.[34] For this study, 45 confocal mosaics were blindly evaluated for the presence (or absence) of BCC tumors by two clinicians: a senior Mohs surgeon with several years' experience and expertise in interpreting confocal images and a novice Mohs fellow with limited few months of experience. BCCs (all subtypes) were detected with an overall high sensitivity and specificity of 96.6% and 89.2%, respectively. The negative predictive values (NPV) were 98.4% for the senior (expert) Mohs surgeon and 91.9% for the novice. A relatively lower NPV reported by the novice reader was the result of lack of experience in evaluating confocal

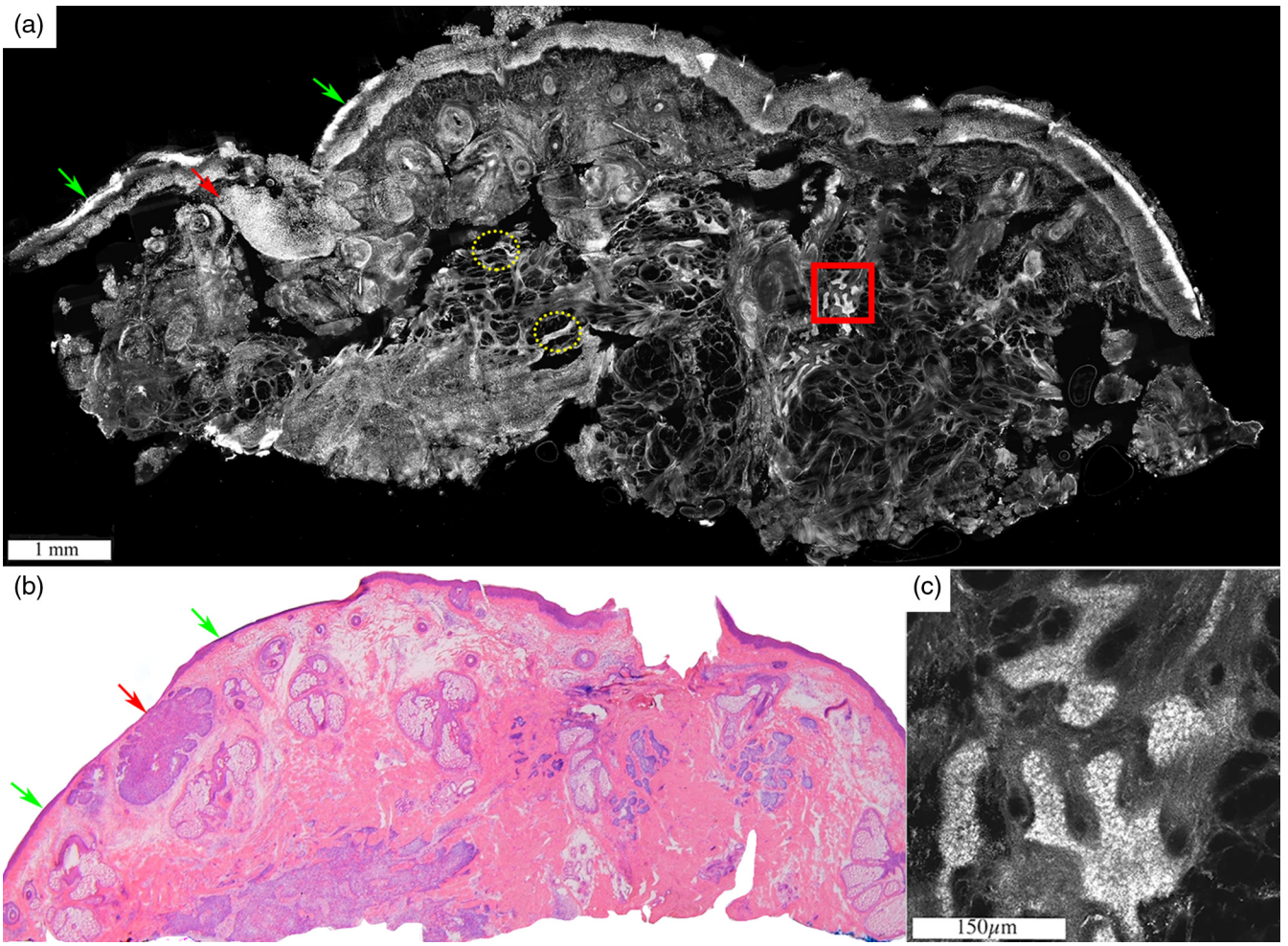

Fig. 2 Acetic acid stained reflectance confocal mosaic (a) shows nodular and infiltrative BCCs and (b) corresponding H&E stained frozen histology. Tiny strands of infiltrative BCC (red boxed area) are difficult to identify and differentiate from thin bright strands of collagen fibres (yellow dotted circles) at low magnification in contrast to the nodular BCC (red arrow) that appears distinct (a). (c) Digital zooming to 30× magnifications is often required to identify the tiny strands of infiltrative BCC. The epidermal margin (green arrows) is seen. Scale bars: A = 1 mm; C = 150 μm. Figure reproduced with permission, courtesy of Wiley.[15]

images. Several interesting outcomes were drawn from this study.[34] Detection of superficial BCC was most challenging in the absence of adjacent epidermal margins, which is probably related to the incomplete or uneven flattening of the epidermis in the tissue mounting device. Flattening of the edges of Mohs surgical excisions is critically necessary when preparing frozen sections to allow viewing of the complete epidermal margins (Fig. 6).[34]

Identification of infiltrative BCC was relatively easy when present as multiple tumor clusters, however, remained relatively challenging when there were only few clusters, as reported previously (Fig. 3).[14]

This study also demonstrated the existence of a learning curve for reading FCM images as well as the bias of previous history of training and experience on reading accuracy. The expert Mohs surgeon was highly sensitive (98.9%), but historical experiences also led to somewhat conservative and cautious reading for absence of residual tumor, resulting in relative lower specificity (83.3%). By comparison, the novice was not as accurate in detecting the presence of tumor and was relatively less sensitive (94.4%) but the shorter historical experience led to relatively bolder reading for absence of tumor, resulting in relatively higher specificity (95.0%). Some technical challenges were also highlighted such as the need for improving mosaicking speed while maintaining image quality, as well as for building inexpensive and user-friendly equipment for increased acceptance of this technology in clinical realms. (While the current speed of mosaicking is certainly faster by more than ~2× than the time taken in current surgical practice to prepare frozen sections, this time does not include the time taken for sample preparation, which includes acridine orange-staining followed by mounting and flattening of tissue. Moreover, multiple excisions (2 or more) are often taken during a single Mohs surgical procedure. For these reasons, further improvement in mosaicking speed will help toward wider acceptance and adoption of the CMM approach.

2.2 *Confocal Mosaicking Microscopy Imaging from Bench to Bedside*

The laboratory work, along with the advent of a second generation commercialized smaller and faster microscope (VivaScope^{R} 2500,

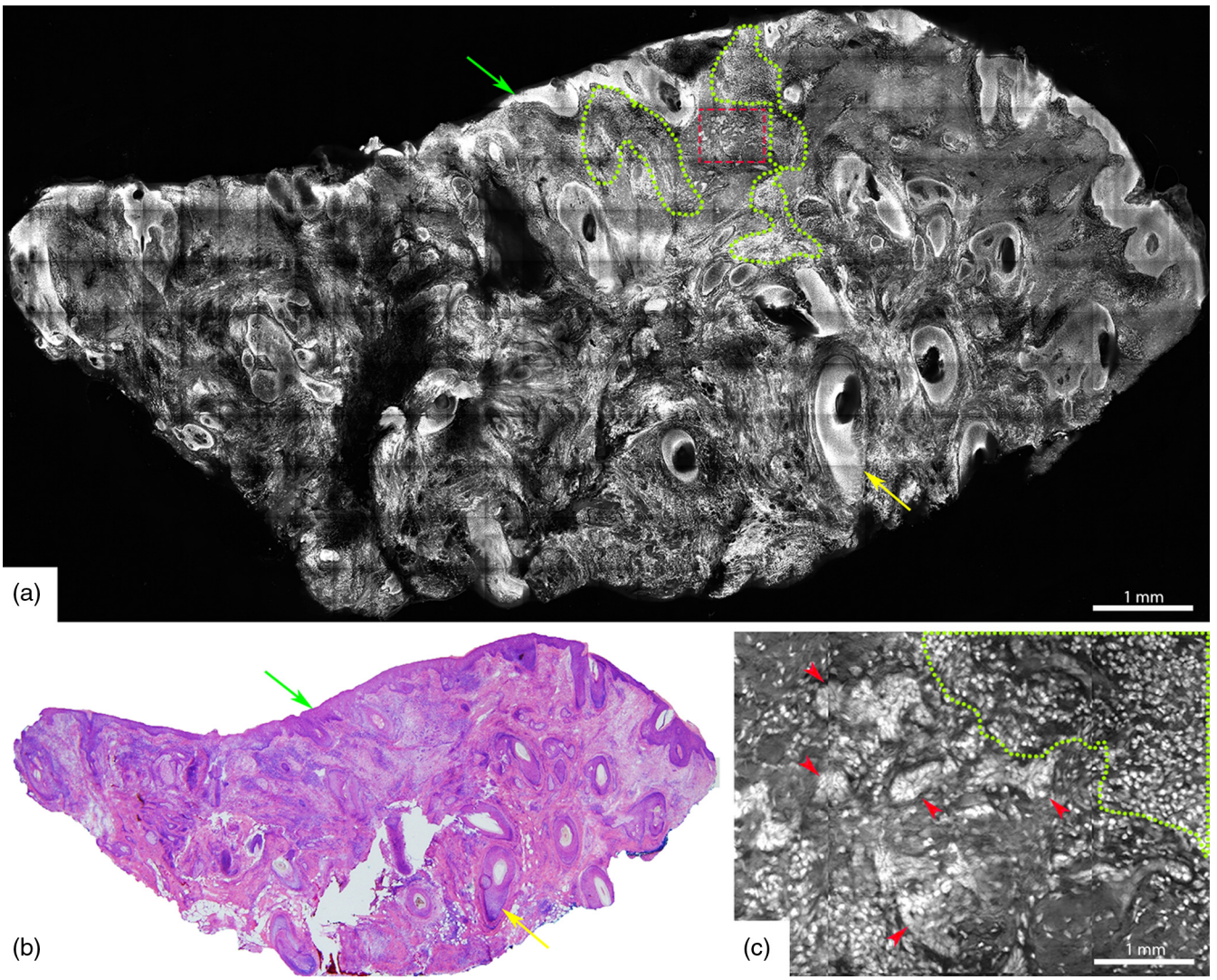

Fig. 3 Low tumor volume of infiltrative BCC can be readily detected on a wide-field fluorescent confocal mosaic. Acridine orange stained fluorescence confocal mosaic (a) shows a small focus of residual infiltrative BCC (dashed red box) as bright strands that can be identified within the reticular dermis even at this low magnification, corresponding to 2× magnification on (b) H&E-stained frozen histopathology. However, it can sometimes be challenging to differentiate these particularly thin tumor strands (four to eight cells thick; dashed red box) from the surrounding inflammatory infiltrate (green dotted circles) and may require digital zooming to higher magnification (4× to 10×). (c) Submosaic shows digital zooming of the area under the red dashed box from mosaic "A" necessary to appreciate pleomorphic nuclei and enlarged nuclear cytoplasmic ratio of the tumor strands (red arrowheads) and differentiate them from bright smaller monomorphic inflammatory cells (green dotted circles). Epidermis (green arrow) and hair follicle (yellow arrow) are seen. On a separate note, the dark bands that are seen in this particular mosaic (but not the others shown in this paper) are due to incomplete correction for the illumination fall-off (vignetting) that occurs across each image and incomplete stitching along the edges of images. This was merely due to the developmental state of the stitching algorithm and software at the time. (Further development led to a second algorithm that produces much more seamless appearing mosaics, as seen in the other figures.) Scale bars: A, C = 1 mm.

Caliber Imaging and Diagnostics, Rochester, New York), paved the path for FCM-acridine orange testing in actual clinical and Mohs surgical settings directly on fresh excised tissue (instead of discarded frozen-thawed tissues that was used in the laboratory development work).

Bennassar et al.[28] were the first group to advance FCM to testing and use at the bedside. Fresh tissues from shave biopsies were obtained from two whitish facial papules in two different patients with equivocal dermoscopic diagnosis. The biopsies were stained with acridine orange and imaged with FCM. A diagnosis of intradermal nevi (IDN) and infiltrating BCC, respectively, was reached from the FCM images within 170 s of tissue excision. Immediate point-of-care clinical management was feasible in both cases, based on the results of FCM imaging alone. In case of IDN, electrodesiccation of the wound base was performed without causing much harm to the tissue. For BCC, Mohs surgery was performed in the same setting, resulting in total tumor clearance. FCM diagnosis correlated well with their corresponding histopathology. This report, for the first time, demonstrated the feasibility of performing FCM-acridine orange

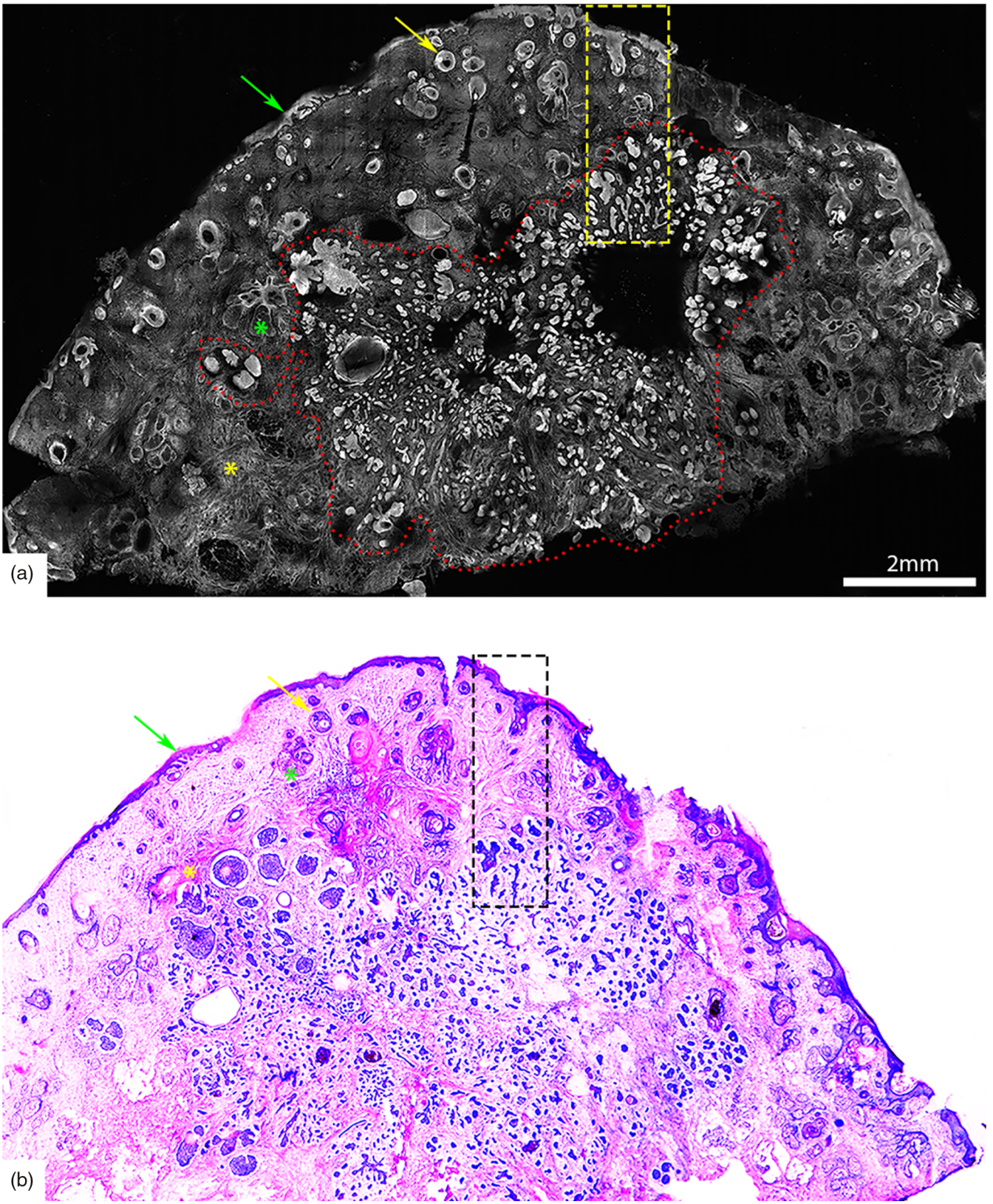

Fig. 4 Acridine orange stained fluorescence confocal mosaic of a micronodular BCC (a) that equates well to 2× view on standard H&E stained histology section (b). Small and tiny nodules or nests of tumor (red dotted area) can be identified at this magnification. Epidermis (green arrow), hair follicle (yellow arrow), sebaceous glands (green asterisk), dermal collagen (yellow asterisk) are seen. Scale bar: A = 2mm. Figure reproduced from Gareau et al. "Confocal mosaicing microscopy in Mohs skin excisions: feasibility of rapid surgical pathology."[14]

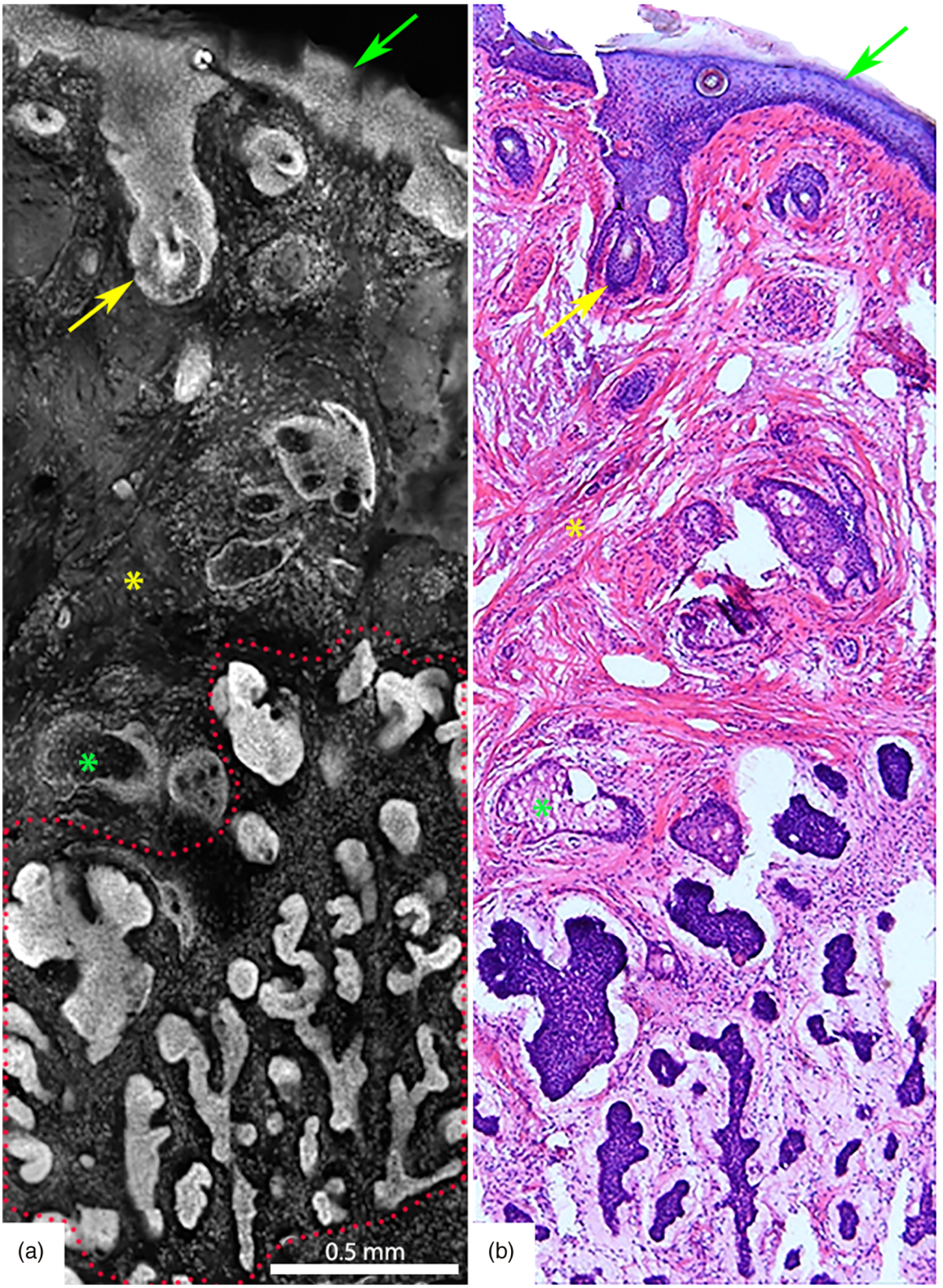

Fig. 5 Acridine orange stained fluorescence confocal submosaic (a) obtained by digitally zooming (6× magnification) in the mosaic (Fig. 4(a), dashed boxed area) to appreciate morphological features of micronodular BCC tumor (red dotted area) such as nuclear pleomorphism, increased nuclear density, and clefting. Epidermis (green arrow), hair follicle (yellow arrow), sebaceous glands (green asterisk), dermal collagen (yellow asterisk) are seen. This corresponds well with H&E stained frozen histopathology (b). A = 0.5 mm. Figure reproduced from Gareau et al. "Confocal mosaicing microscopy in Mohs skin excisions: feasibility of rapid surgical pathology."[14]

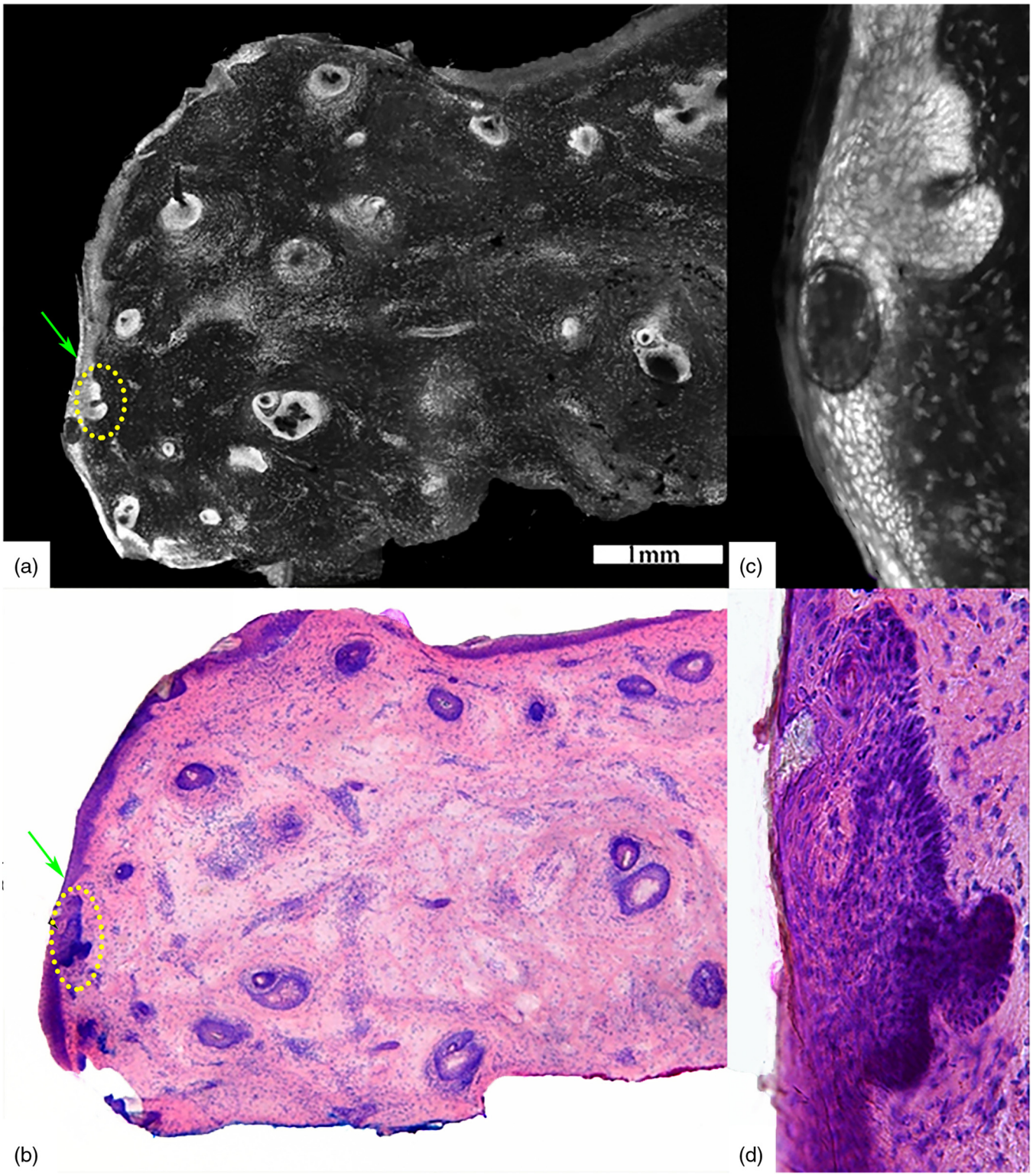

Fig. 6 (a) Acridine orange stained fluorescence confocal submosaic shows a small bright focus (dotted circle) of superficial BCC along the epidermal margin (green arrow) raising suspicion for residual tumor and (b) corresponding H&E-stained frozen histopathology at 4× magnification. Digital zooming to higher magnification (30×) reveals the subtle but characteristic features of (c) superficial BCC on confocal image as well as on (d) H&E-stained frozen histopathology. This figure demonstrates that small foci of superficial BCC may be sometimes missed on confocal imaging either due to their subtle morphological features or uneven flattening of the tissue. Scale bar: A = 1 mm. Figure reproduced with permission, courtesy of Wiley.[34]

mosaicking rapidly and reliably in an actual clinical setting for the evaluation of fresh *ex vivo* tissues.

Later, Bennàssar et al.[29] advanced the implementation and testing of FCM imaging in clinics by defining FCM criteria for all subtypes of BCC. This was a quintessential step to improve the reproducibility of BCC diagnosis and its differentiation from surrounding dermis and adnexal structures (especially small hair follicles) that often pose diagnostic dilemma. Sixty-nine tumor samples from 66 patients were obtained as 1-mm strips from the first Mohs stage excision without disrupting the tissue margins for ulterior frozen section assessment. FCM mosaics were acquired and evaluated by the attending Mohs surgeon, experienced in analyzing both frozen sections and FCM images in the operating room in real time. Tissues were subsequently submitted for histopathological evaluation.

Broadly, the tumors were classified as either superficial BCC (sBCC), nodular (nBCC), or micronodular-infiltrative BCC (iBCC) (Fig. 7 and Table 1). Eight morphological-fluorescent criteria were defined for BCC, including presence of fluorescence, clear demarcation, nuclear crowding, clefting, nuclear pleomorphism, palisading, increased nuclear cytoplasmic (N/C) ratio, and the presence of stromal reaction (Fig. 7 and Table 1). Of these, hyperfluorescent aggregates with nuclear crowding (91%), palisading (96%), and nuclear pleomorphism (100%) were identified in all subtypes of BCCs. However, certain criteria were more pronounced than others, which aided in subtyping of BCC. For example, sBCCs appeared poorly defined with hyperfluorescent structures (tumoral nuclei) sparsely distributed along the basal layer of the epidermis with surrounding clefting [Fig. 7 and Table 1]. Stromal reaction and inflammation was less prominent in sBCCs. On the contrary, nBCCs appeared as well-demarcated nodules with crowded hyperfluorescent pleomorphic nuclei, peripheral palisading, and clefting [Fig. 7 and Table 1]. Unlike sBCCs, a significant stromal "starry sky" pattern was associated with nBCCs. Likewise, iBCCs were described as nests and strands of hyperfluorescent pleomorphic nuclei infiltrating dermis with variable nuclear crowding, palisading, and clefting [Fig. 7 and Table 1]. Strong stromal and inflammatory reaction was the most prominent feature of iBCCs [Fig. 7 and Table 1]. FCM criteria, such as clefting, palisading, and "starry sky" stroma, had high specificity for BCC detection and were useful in differentiating BCC nests from the surrounding adnexal structures. The authors stressed the importance of "starry sky" stroma that should initiate a thorough search of BCC foci in the absence of tumor nests. The outcome of the FCM mosaics analysis was later compared with the results of H&E slides. The comparisons were independently evaluated by a dermatopathologist and demonstrated high overall concordance ($\kappa = 0.9$) in classifying BCC subtypes.[29] In order to further validate the aforementioned FCM criteria, the same FCM images were also independently evaluated by two dermatologists. These criteria were validated with κ values greater than 0.7 for most criteria in both independent observers.

Recently, Bennàssar et al.[30] conducted another study, in the Mohs surgical setting, where—for the first time—true surgically excised fresh tissue margins from 80 BCC lesions (with or without tumors) were prospectively imaged with FCM. The goals of this study were (a) to evaluate the sensitivity and specificity of *ex vivo* FCM imaging in detecting residual BCC in Mohs tissue excisions and (b) to calculate the time invested up to the diagnosis for both FCM and frozen sections. The attending Mohs surgeon evaluated mosaics in the operating room in real time for the presence or absence of BCC, especially at the lateral margins. The reading of the FCM mosaics also mimicked the usual frozen section slide-reading process during Mohs surgery, as described previously. Later, frozen pathology was independently evaluated by a dermatopathologist in a blinded manner.

The results of both FCM and frozen section were compared and an overall high sensitivity and specificity of 88% and 99%, respectively, of detecting BCC was found. Their result[30] is on par with and validates the results of the initial studies.[34] Micronodular/infiltrating BCC was the main histological subtype in this study. The diagnosis of BCC was missed in 10 cases, which were later confirmed as infiltrating BCC with thin strands (two to three cell layers) of tumor cells on frozen section. This misdiagnosis was attributed to either the lack of sufficient training for the Mohs readers or to the differences in the level of tissue section examined: surface imaging of true margin by FCM but deeper subsurface frozen sections. Only one false-positive margin was reported in this study, making FCM a highly specific tool for detection of tumor margins in fresh tissues. However, the main limitation of this study was low prevalence of positive margins for BCC, making the results of high positive predictive value and NPV of 98% and 97%, respectively, less reliable. This study also proved that FCM markedly reduces the time of tissue preparation and evaluation by almost two-thirds, in comparison to traditional method of frozen sections.

Following the initial reports from Barcelona, Longo et al.,[31] published a case report of recurrent BCC that was subjected to FCM-acridine imaging for margin control using Mohs surgery. The lesion was excised under local anesthesia without surgical debulking and then the excised tissue was sliced into several smaller samples to evaluate margins. The time required to image all samples was about 9 min. The infiltrative type of BCC was clearly identified in the deeper margin and correlated well with corresponding frozen section diagnosis. In this particular case, the patient refused further surgery and was subsequently treated with intensity modulated radiation therapy. This study highlights the potential role of FCM mosaicking in the management of complex and recurrent tumors.

2.3 *Translation of Confocal Mosaicking Microscopy Guided Mohs Technology Platform to Other Perioperative Settings*

2.3.1 *For the evaluation of melanocytic lesions*

Although the role of frozen sections for intraoperative margin assessment of BCC and SCC is well established, it remains controversial for the management of malignant melanoma.[35] Frozen sectioning may cause artifacts due to freezing and sectioning of tissue, hindering the assessment of intraepidermal spread of melanocytes (pagetoid cells) in early melanoma and depth of invasion (of paramount importance for management and prognosis) on subsequent histopathology.[35] When Mohs surgery is used for melanoma, immuno stains are frequently utilized to facilitate margin assessment especially in melanoma of the lentigo maligna type with unpredictable subclinical extent.[36] Thus, in the absence of intraoperative histological feedback during malignant melanoma (MM) resection, surgeons take wide resection margins (5 to 10 mm) to ensure complete

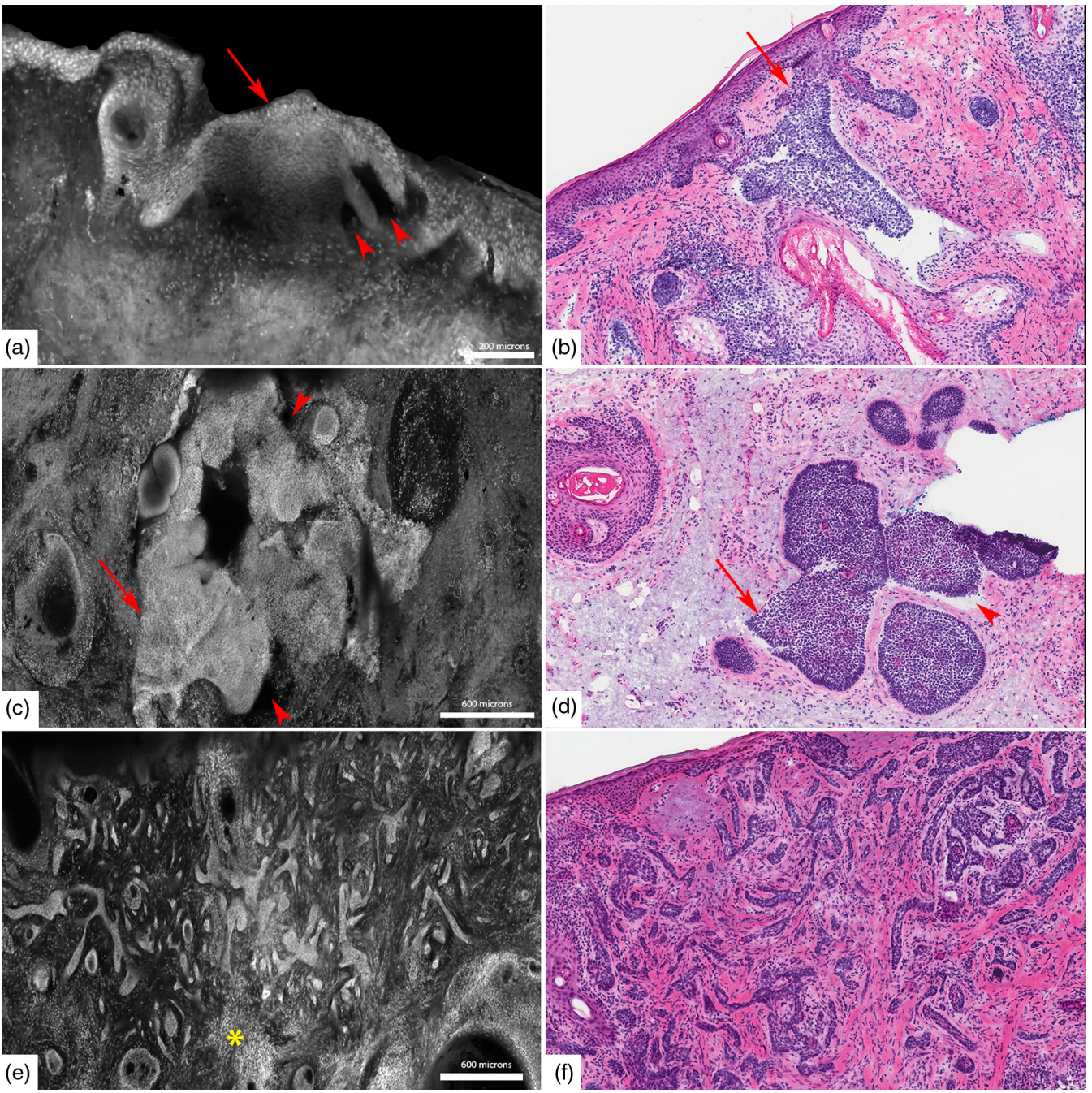

Fig. 7 Fluorescent confocal microscopy criteria for various subtypes of BCCs. (a, c, e) Submosaics show characteristic morphological features of BCCs: presence of fluorescence, nuclear pleomorphism, increased N/C ratio, and palisading in (a) superficial BCC, (c) nodular BCC, and (e) infiltrative BCC. The tumor islands (red arrows) are well demarcated in (c) nodular BCC and (e) infiltrative BCC than the (a) superficial BCC, whereas clefting (red arrowheads) appears more prominent in superficial BCC (a) and nodular BCC (c). (e) "Starry sky" (yellow asterisk) appearance of the tumor stroma is pronounced in infiltrative BCC. (b, d, f) And corresponding H&E-stained frozen histopathology (10×). Scale bars: A = 200 μm; C & E = 600 μm.

tumor clearance, making tissue-sparing surgery especially challenging in the cosmetically important parts of the face. *In vivo* RCM has shown high sensitivity (91% to 97%) and specificity (68% to 86%) of detecting melanoma.[37] Melanin pigment has a high reflectance on RCM enabling identification of intraepidermal pagetoid cells without the use of an exogenous contrast agent. Furthermore, since the imaging does not require tissue processing, it does not interfere with the assessment of the depth of invasion on subsequent histopathology. Therefore, *ex vivo* RCM could be a valuable rapid intraoperative tool for the diagnosis and management of melanocytic lesions especially melanoma of the lentigo maligna type.

Here, we summarize two studies in which *ex vivo* RCM has been explored for imaging melanocytic lesions in an intraoperative setting. Debarbieux et al.[38] were the first to assess the feasibility of performing imaging on nail matrix during

Table 1 FCM criteria for BCC and their subtypes.[29]

FCM criteria and p value[a] for subtyping BCCs	sBCC	nBCC	iBCC	Definition of FCM criteria
Presence of fluorescence (<0.01)	3+	3+	3+	Nucleated cells stained with acridine orange
Well demarcated (<0.01)	1+	3+	2+	Separation of tumor border from surrounding stroma
Nuclear crowding (0.60)	1+	3+	3+	Nuclear density higher than surrounding epidermis and adnexal structures
Nuclear pleomorphism (0.80)	3+	3+	3+	Deviation from normal round-oval nuclear outline of normal keratinocytes
Increased N/C ratio	3+	3+	3+	Elongated heterogeneous fluorescent (spots) nuclei with poor/absent cytoplasm
Palisading	3+	3+	3+	Peripheral polarized aligned fluorescent ellipses: outermost row of basal cells
Clefting (<0.01)	3+	3+	2+	Black fluorescence-free half-moon attached to the tumor mass
Tumor stroma				Densely nucleated dermis reminiscent of a "starry sky"
Absent (<0.05)	2+	1+	1+	
<50%	2+/3+	1+	2+	
>50%	1+	3+	3+	

Note: iBCC, infiltrating BCC; nBCC, nodular BCC; sBCC, superficial BCC; N/C ratio, nuclear-to-cytoplasmic ratio. The numbers 1+, 2+, 3+ indicate the relative frequency with which the FCM features were present in a particular subtype of BCC.
[a]Statistically significant differences between BCC subtypes in demarcation, nuclear crowding, clefting, and stroma are shown.

surgical procedure. Currently, the diagnosis of suspected subungual melanoma requires a biopsy of the nail matrix for histopathological confirmation[38] followed by a second surgical procedure at a later time for the treatment. However, if the lesion is benign, the ensuing permanent nail dystrophy from biopsy of the nail matrix can be upsetting to the patient. This study included nine patients, who underwent a matricial biopsy for an acquired melanonychia (one benign lentigo and eight melanomas). RCM imaging was performed *in vivo* on the nail matrix either after reclination of the nail plate, or *ex vivo* on the fresh tissue biopsy, or both. RCM revealed sufficient cytological and architectural features to accurately identify melanoma (including melanoma *in situ*) and differentiate it from benign melanocytic lesions. Results were comparable with final histopathological diagnoses. Thus, by providing extemporaneous diagnosis of subungual melanoma, RCM could enable one-step point-of-care surgical treatment on the very same day.

Later, Cinotti et al.[39] used a similar approach, combining *in vivo* and *ex* vivo RCM imaging for the diagnosis and management of a case with an eyelid margin MM. Typical features indicative of a diagnosis of MM, which include disarranged epithelium with large hyper-reflective dendritic and roundish pagetoid cells in the superficial chorion as well as invading the eyelash follicles, were identified using *in vivo* RCM, which then led to the surgical excision of the lesion. The excised tissue was immediately evaluated by *ex vivo* RCM for the tumor margin clearance, providing the diagnosis and surgical closure in a single setting, obviating the need for a prior biopsy. Although these two studies have shown the utility of RCM imaging in the diagnosis and management of MM, further studies involving validation on larger sample sizes are needed to bring this technology into routine surgical workflow.

2.3.2 *For the evaluation of squamous cell carcinomas and other neoplasms*

Ex vivo confocal microscopy has recently been explored for the evaluation of SCC and other nonpigmented neoplasms.[40] Debarbieux et al.[40] imaged fresh biopsies from 10 cases with nonpigmented tumors of nail matrix with *ex vivo* FCM. This included two invasive and three benign epithelial tumors, four *in situ* or minimally invasive SCC, and one nodular amelanotic melanoma. Confocal mosaics were evaluated in real time and retrospectively compared with H&E sections. Clinically acceptable correlation was exhibited by malignant epithelial tumors (Bowen disease, invasive SCC, and onycholemmal carcinoma) but poor for *in situ* or minimally invasive SCC and for nodular melanoma. This study demonstrated that *ex vivo* FCM could be a useful tool to shorten the management effort and duration for nonpigmented malignant tumors because the surgeon can perform wide excision within the same procedure without waiting for a biopsy report. Similar studies involving larger sample sizes of nonpigmented tumors, especially benign epithelial tumor and amelanotic melanoma, are required for its actual clinical application.

2.3.3 *For the evaluation of infectious diseases*

Recently, Leclercq et al.[41] reported two cases, where *ex vivo* RCM was used to diagnose cutaneous mucormycosis, a life-threatening fungal infection that occurs in immunocompromised patients. Images were acquired in both reflectance and fluorescence mode. Mucormycetes appeared as hyper-reflective elongated structures (20 μm in diameter) with perpendicular ramifications. The results were comparable to conventional histopathology. The diagnosis of mucormycosis relies on direct examination of skin scraping under conventional light microscopic and histological examination followed by fungal typing

on culture or polymerase chain reaction (PCR). Skin scraping is currently the only rapid method for the detection of fungal infections; however, it not only has low sensitivity but also destroys tissue architecture that impedes further evaluation. *Ex vivo* RCM has the advantages of both being fast, as with the direct light microsopic examination, and the ability to localize fungi in intact tissue, as with the histological examination, to increase the sensitivity of fungal typing on PCR. The imaging allowed to rapidly confirm the clinical diagnosis of mucormycosis, which is essential for the treatment of this fungal infection. Further studies are necessary to compare the performance of *ex vivo* RCM with the findings of conventional histological and mycological examinations.

2.4 *Current Limitations of Confocal Mosaicking Microscopy and Future Advancement Toward Clinical Translation*

All of the studies to date provide compelling evidence of FCM's translational potential to expedite *ex vivo* evaluation of fresh tissue for the detection of residual BCC in Mohs surgical margins and potentially other clinical applications. Nonetheless, these studies also highlighted limitations that will need to be overcome to integrate FCM into routine clinical workflow. Here, we list some of these limitations and their potential solutions.

2.4.1 *Technical limitations*

FCM evaluation of Mohs surgical margins could benefit by improving contrast and specificity, and obtaining seamless mosaics, with more consistently flattened imaging surface showing the complete epidermal margins. Better contrast and specificity could help enhance the detection of otherwise missed thin strands of infiltrative and sclerosing BCC tumors. To increase the contrast, especially for thin and tiny tumors, one could use more specific markers. Anti-BerEP4-antibody is one such tumor marker that has been shown to specifically stain BCC tumor cells on thin formalin fixed sections.[42] Later on, the same group showed the feasibility of a macro-/micro-optical system to image the expression of BerEP4 on cultured cancer cells (SW620, a BerEP4-expressing cell line) in three dimensions.[43] However, to best of our knowledge, anti-BerEP4-antibody has not yet been described on fresh tissue, and it would be interesting to explore such molecules or similar molecules for *ex vivo* CMM.

Multimodal imaging approaches, such as a combination of CMM with multiphoton microscopy (MPM), could also improve the detection of thin tumor strands. CMM could rapidly evaluate large areas of fresh tissue to flag areas that may contain thin tumor strands, whereas MPM could evaluate these flagged areas at a much higher and specific contrast to confirm the presence or absence of tumor. In addition, on MPM, thin tumor strands would be better delineated from their surrounding collagen tissue due to differences in the tissue signal:[44] autofluorescence from cells and second harmonic generation from collagen,[45] which could be especially beneficial for the detection of sclerosing BCC.

Likewise, faster speed of acquiring images and better stitching of mosaics could further expedite the Mohs surgery procedure. (The need for continued improvement in speed was explained earlier, at the end of Sec. 2.1.) Recently, Abeytunge et al.[32] described a new acquisition and stitching technique called strip mosaicking confocal microscopy that can seamless display 10 mm × 10 mm in <3 min, potentially offering a means for real-time bedside pathology. Larson et al.[46] tested this approach on 17 Mohs surgical excisions (BCCs and SCCs) and showed an overall clinically acceptable image quality in terms of resolution, contrast, and stitching, along with high sensitivity and specificity of 94% for detecting skin cancer margins. This technique is currently being adapted for commercialization of a new version of a CMM device. However, this new device needs to be validated in clinical settings with a larger samples size of both BCCs and SCCs, before being integrated in the Mohs surgical workflow.

Previous studies have also highlighted incomplete or uneven flattening of skin tissue excisions as one of the causes of missed diagnosis of sBCC.[34] Efforts are ongoing to build a refined tissue mount system that could be used specifically for flattening large excisions of hard tissues such as skin. Recently, Cinotti et al.[47] described a new "tissue press" device to flatten fresh tissue for *ex vivo* confocal microscopy examination. This device was tested on 10 skin samples, where complete mosaic images were achieved. Furthermore, it was confirmed that this device did not damage tissue for subsequent histopathological evaluation.[47]

2.4.2 *Lack of trained readers*

Based on the above studies, it is evident that very few clinicians are currently well versed in reading FCM mosaics and expertise is limited to academic centers. In order to integrate FCM in the clinical workflow, there is a need to expand the existing pool of readers. Three workshops have been held, and, currently, some courses are being organized on an annual basis for Mohs surgeons. However, such courses should also be introduced to residents and fellows in dermatology and dermatopathology and Mohs surgery fellowships early in their career to support wider acceptance and adoption.

2.4.3 *Learning Curve*

Another reason for the lack of readers is the reluctance of trained clinicians to learn to interpret grayscale (black-and-white) confocal mosaics instead of more familiar purple and pink appearing images of histopathology. To address this barrier, an advanced multimodal-digital staining approach is being developed to recreate images that appear similar to conventional purple-and-pink appearance of H&E images.[48,49] This approach simultaneously images tissue in both fluorescence (FCM) and reflectance (RCM) modes. Images acquired in fluorescence contrast highlight only nuclei and can thus be digitally colored purple (this simulates hematoxylin staining component of H&E), whereas those acquired in reflectance contrast highlight only cellular cytoplasm and dermal morphology and can thus be digitally colored pink (this simulates eosin staining component of H&E Figs. 8 and 9).

Overlaying the two on each other produces purple and pink colored confocal mosaics. Gareau et al.[49] developed and tested this approach on 35 BCC excisions, stained with acridine orange, from Mohs surgery in a preclinical study and showed good correlation with the H&E stained frozen pathology. Recently, the same group conducted a retrospective study to assess the potential of digitally stained confocal mosaics (DSCMs) for screening SCC and BCC in Mohs excisions.[50] For this, 133 DSCMs from 64 Mohs discarded tissue excisions were evaluated by three Mohs surgeons in a blinded manner,

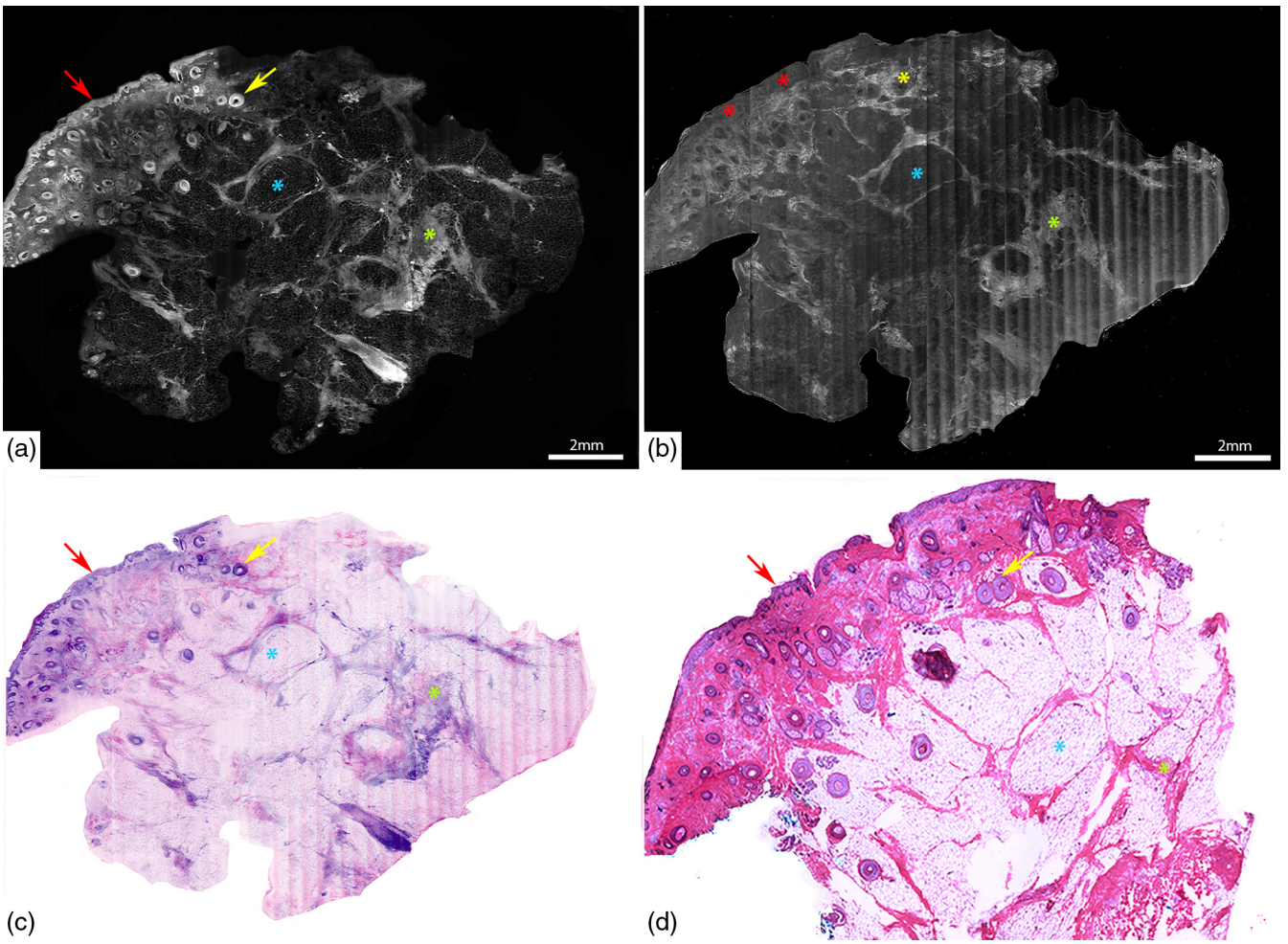

Fig. 8 DSCMs of normal skin tissue closely mimicking H&E stained tissue histology. Mosaic of normal skin tissue in (a) fluorescence mode, (b) in reflectance mode, and (c) digital H&E (DHE) image created by overlapping fluorescence and reflectance channels. Nucleated structures, such as epidermis (red arrows) and hair follicle (yellow arrow), appear bright in fluorescence mode (a) and dull-grey on reflectance mode (b). Adipocytes (blue asterixis) appear darker and well defined in the fluorescence mode than in reflectance mode. By contrast, dermal collagen (green asterixis) appears bright in both the modes. (d) The H&E image (2×) compares well with the DHE image (c). Scale bars: A, B = 2 mm.

before and after brief training. They demonstrated average respective sensitivities and specificities of detecting NMSC of 90% and 79% before training and 99% and 93% after training. There was also a significant increase in the interobserver agreement from 72% pretraining to 98% ($\kappa = 0.97$; $P = 0.04$) posttraining. They also noted a marked reduction of training time to 5 min as compared to traditional grayscale confocal microscopy that requires a training period minimum of 30 min with at least 2 months of confocal imaging experience.[34,48] However, the appearance of the mosaics remains somewhat variable in quality, due to artifacts from acridine orange staining in the presence of tissue heterogeneity, mainly saturation in nuclei and/or residue in the dermis. This approach still needs optimization and larger scale validation studies before it could actually be implemented into regular clinical workflow.[49]

2.4.4 *Lack of data on the detection of squamous cell carcinoma*

Although FCM has shown high sensitivity and specificity of detecting all subtypes of BCC tumors, similar studies are lacking to determine the role in the detection of SCC in Mohs surgical margins. Longo et al.[51] recently showed preliminary data, where only cutaneous SCC lesions from Mohs surgery were imaged with FCM-acridine orange. A total of 47 mosaics from 13 lesions were evaluated for the presence or absence of SCC in fresh tumor sections and margins. Attempts were made to further grade SCC as "well," "moderately," or "poorly" differentiated based on five features: fluorescence, tumor silhouette, keratin pearls, nuclear pleomorphic, and keratin formation. Only one case of *in situ* SCC was missed, and one margin showed false positivity.[51] This study showed the feasibility of identifying and grading SCC with FCM-acridine orange in Mohs surgical margins. However, similar studies on larger sample sizes, including all grades of SCC, are needed to validate the potential role of FCM in the diagnosis of SCC in the clinical setting.

2.4.5 *Reimbursement barrier in USA*

Finally, another limitation to ready acceptance and adoption of *ex vivo* CMM in clinical settings especially in the USA is the current lack of reimbursement codes. Current procedural terminology (CPT) reimbursement codes were recently granted for RCM for cellular and subcellular imaging of skin; image

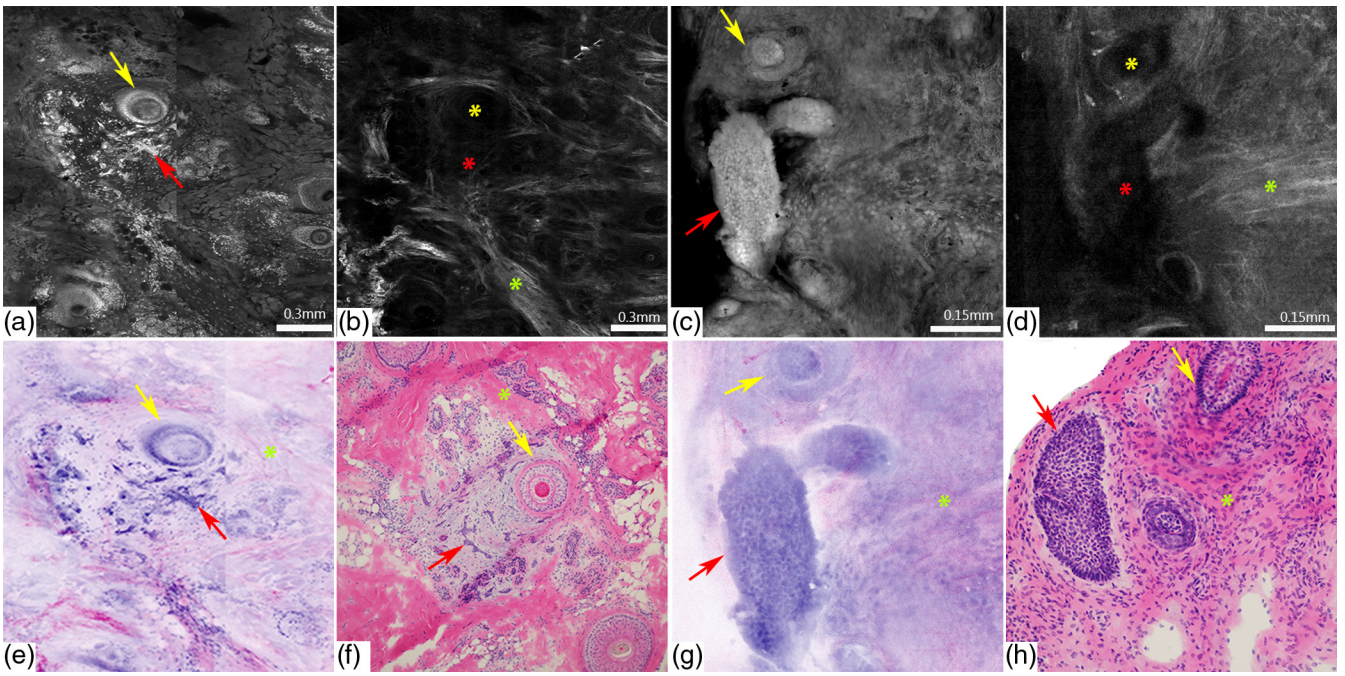

Fig. 9 DSCMs of BCCs closely mimicking H&E stained tissue histology. Submosaics shows (a, c) infiltrative BCC and nodular BCC in fluorescence mode, (b, d) in reflectance mode, and (e, g) digital H&E (DHE) images created by overlapping fluorescence and reflectance channels, respectively. (a, e) Nucleated structures, such as hair follicle (yellow arrows) and tumor cords and nodules (red arrows), appear bright in fluorescence mode and (b, f) are not visible (yellow and red asterixis) on reflectance mode. By contrast, dermal collagen (green arrows) appears more pronounced in the reflectance mode bright in (b, f; green asterixis). Corresponding H&E images of (f) infiltrative and (h) nodular BCC at 10× magnification compares well with the DHE images (d and g, respectively). Scale bars: A, B = 0.3 mm; C, D = 0.15 mm.

acquisition and interpretation and producing a report. However, these codes are currently only applicable for reflectance contrast and for imaging *in vivo*.[52] Thus, for successful integration of CMM guided Mohs surgery, similar CPT codes would also be necessary for imaging *ex vivo* tissue. However, to receive such codes, multicenter studies will need to be performed, showing appropriate levels of evidence for accuracy. This, obviously, remains a longer-term proposition.

3 Conclusion

Despite some technical limitations, CMM appears to be clearly promising for detection of residual BCC tumor margins in fresh Mohs surgical excisions. Early adopter Mohs surgeons have reported high sensitivity (89% to 96%) and high specificity (99% to 89%) in six reasonably large studies, involving reasonably large numbers (17 to 80) of tissue specimens.[53] The consistency of these results across diverse settings (New York, Barcelona, Modena) suggests that the current technical limitations (mainly consistency for tissue flattening, uneven stitching, and irregular contrast agent uptake), although yet to be fully resolved, may ultimately have relatively minor-to-small impact on the overall ability and utility of this approach to offer a means to perform rapid pathology in fresh tissue. In at least three studies, senior Mohs surgeons with a lot of experience and expertise in reading confocal mosaics were able to train junior surgeons (and confocal imaging novices) in a matter of few months. Possibly, this reflects two advantages: one, the use of a nuclear-specific contrast agent in excised tissue, and second, particularly in Mohs settings, frozen pathology sections are prepared and read in the en face orientation, which is the same as that of confocal mosaics. Both advantages result in a one-to-one correspondence between the nuclear morphologic patterns and dermal features seen in the mosaics and those in the pathology, which, consequently, appears to facilitate a reasonably quick learning curve for reading mosaics. Of course, the grayscale contrast still remains a disadvantage, but this is being addressed by the approach of digital colorizing of the combined fluorescence-and-reflectance mosaics. Once the current technical limitations are addressed, the next phase of research will be necessarily aimed at further validation in larger trials. Finally, as we are seeing already, the early work in BCCs and the Mohs surgical setting for BCCs will pave the way for similar applications in other skin lesions and in tissues in other settings.

Disclosures

Milind Rajadhyaksha is a former employee of, and owns equity in, Caliber Imaging and Diagnostics (formerly, Lucid Inc.), the company that manufactures and sells the VivaScope confocal microscope. The VivaScope is the commercial version of an original laboratory prototype that was developed by Rajadhyaksha when he was at Wellman Laboratories of Photomedicine, Massachusetts General Hospital, Harvard Medical School. No conflicts of interest declared for Manu Jain and Kishwer Nehal.

Acknowledgments

We acknowledge Sanjee Abeytunge and Gary Peterson for their technical assistance in acquisition of CMM images, Kivanc Kose for help with preparing images and figures; Marie A. Tudisco

and Phillips, William H. for providing tissue and preparing frozen sections and Sri. Varsha Pulijal for scanning the H&E slides. The research at MSKCC was supported by grants from the Byrne Fund and the NIH (R01EB002715, R01EB012466 and, in part, by P30CA008748).

References

1. H. W. Rogers et al., "Incidence estimate of nonmelanoma skin cancer (keratinocyte carcinomas) in the U.S. population, 2012," *JAMA Dermatol.* **151**(10), 1081–1086 (2015).
2. S. V. Mohan and A. L. Chang, "Advanced basal cell carcinoma: epidemiology and therapeutic innovations," *Curr. Dermatol. Rep.* **3**, 40–45 (2014).
3. P. S. Karia, J. Han, and C. D. Schmults, "Cutaneous squamous cell carcinoma: estimated incidence of disease, nodal metastasis, and deaths from disease in the United States, 2012," *J. Am. Acad. Dermatol.* **68**(6), 957–966 (2013).
4. J. T. Chen, S. J. Kempton, and V. K. Rao, "The economics of skin cancer: an analysis of medicare payment data," *Plast. Reconstructive Surg. Global Open* **4**(9), e868 (2016).
5. M. R. Donaldson and B. M. Coldiron, "No end in sight: the skin cancer epidemic continues," *Semin. Cutaneous Med. Surg.* **30**(1), 3–5 (2011).
6. K. V. Viola et al., "Mohs micrographic surgery and surgical excision for nonmelanoma skin cancer treatment in the Medicare population," *Arch. Dermatol.* **148**(4), 473–477 (2012).
7. L. Ravitskiy, D. G. Brodland, and J. A. Zitelli, "Cost analysis: Mohs micrographic surgery," *Dermatol. Surg.* **38**(4), 585–594 (2012).
8. H. T. Greenway et al., "Microscopic surgery and cutaneous oncology," in *Surgery of the Skin: Procedural Dermatology*, 3rd ed., J. K. Robinson et al., Eds., Elsevier Saunders, China (2015).
9. M. Rajadhyaksha et al., "Confocal examination of nonmelanoma cancers in thick skin excisions to potentially guide Mohs micrographic surgery without frozen histopathology," *J. Invest. Dermatol.* **117**(5), 1137–1143 (2001).
10. Q. L. Erickson et al., "Flash freezing of Mohs micrographic surgery tissue can minimize freeze artifact and speed slide preparation," *Dermatol. Surg.* **37**(4), 503–509 (2011).
11. V. Q. Chung et al., "Use of ex vivo confocal scanning laser microscopy during Mohs surgery for nonmelanoma skin cancers," *Dermatol. Surg.* **30**, 1470–1478 (2004).
12. Y. G. Patel et al., "Confocal reflectance mosaicing of basal cell carcinomas in Mohs surgical skin excisions," *J. Biomed. Opt.* **12**(3), 034027 (2007).
13. M. Y. Al-Arashi, E. Salomatina, and A. N. Yaroslavsky, "Multimodal confocal microscopy for diagnosing nonmelanoma skin cancers," *Lasers Surg. Med.* **39**, 696–705 (2007).
14. D. S. Gareau et al., "Confocal mosaicing microscopy in Mohs skin excisions: feasibility of rapid surgical pathology," *J. Biomed. Opt.* **13**(5), 054001 (2008).
15. D. S. Gareau et al., "Confocal mosaicing microscopy in skin excisions: a demonstration of rapid surgical pathology," *J. Microsc.* **233**(1), 149–159 (2009).
16. A. N. Yaroslavsky et al., "Fluorescence polarization of tetracycline derivatives as a technique for mapping nonmelanoma skin cancers," *J. Biomed. Opt.* **12**(1), 014005 (2007).
17. J. Paoli et al., "Multiphoton laser scanning microscopy on non-melanoma skin cancer: morphologic features for future non-invasive diagnostics," *J. Invest. Dermatol.* **128**(5), 1248–1255 (2008).
18. N. P. Galletly et al., "Fluorescence lifetime imaging distinguished basal cell carcinoma from surrounding uninvolved skin," *Br. J. Dermatol.* **159**, 152–161 (2008).
19. B. Bodanese et al., "Differentiating normal and basal cell carcinoma human skin tissues in vitro using dispersive Raman spectroscopy: a comparison between principal components analysis and simplified biochemical models," *Photomed. Laser Surg.* **28**(Suppl 1), S119–S127 (2010).
20. K. Kong et al., "Diagnosis of tumors during tissue-conserving surgery with integrated autofluorescence and Raman scattering microscopy," *Proc. Natl. Acad. Sci. U. S. A.* **110**(38), 15189–15194 (2013).
21. K. X. Wang et al., "Optical coherence tomography-based optimization of Mohs micrographic surgery of Basal cell carcinoma: a pilot study," *Dermatol. Surg.* **39**(4), 627–633 (2013).
22. J. R. Durkin et al., "Imaging of Mohs micrographic surgery sections using full-field optical coherence tomography: a pilot study," *Dermatol. Surg.* **40**(3), 266–274 (2014).
23. F. B. Legesse et al., "Texture analysis and classification in coherent anti-Stokes Raman scattering (CARS) microscopy images for automated detection of skin cancer," *Comput. Med. Imaging Graph.* **43**, 36–43 (2015).
24. S. Takamori et al., "Optimization of multimodal spectral imaging for assessment of resection margins during Mohs micrographic surgery for basal cell carcinoma," *Biomed. Opt. Express* **6**(1), 98–111 (2015).
25. C. S. Joseph et al., "Imaging of ex vivo nonmelanoma skin cancers in the optical and terahertz spectral regions optical and terahertz skin cancers imaging," *J. Biophotonics* **7**(5), 295–303 (2014).
26. A. Rahman, A. K. Rahman, and B. Rao, "Early detection of skin cancer via terahertz spectral profiling and 3D imaging," *Biosens. Bioelectron.* **82**, 64–70 (2016).
27. A. Gerger et al., "Confocal examination of untreated fresh specimens from basal cell carcinoma: implications for microscopically guided surgery," *Arch. Dermatol.* **141**(10), 1269–1274 (2005).
28. A. Bennassar et al., "Rapid diagnosis of two facial papules using ex vivo fluorescence confocal microscopy: toward a rapid bedside pathology," *Dermatol. Surg.* **38**(9), 1548–1551 (2012).
29. A. Bennàssar et al., "Evaluation of 69 basal cell carcinomas with ex vivo fluorescence confocal microscopy," *JAMA Dermatol.* **149**(7), 839–847 (2013).
30. A. Bennàssar et al., "Ex vivo fluorescence confocal microscopy for fast evaluation of tumour margins during Mohs surgery," *Br. J. Dermatol.* **170**(2), 360–365 (2014).
31. C. Longo et al., "Inserting ex vivo fluorescence confocal microscopy perioperatively in Mohs micrographic surgery expedites bedside assessment of excision margins in recurrent basal cell carcinoma," *Dermatology* **227**(1), 89–92 (2013).
32. S. Abeytunge et al., "Confocal microscopy with strip mosaicing for rapid imaging over large areas of excised tissue," *J. Biomed Opt.* **18**(6), 61227 (2013).
33. J. Bini et al., "Confocal mosaicing microscopy of human skin ex vivo: spectral analysis for digital staining to simulate histology-like appearance," *J. Biomed. Opt.* **16**(7), 076008 (2011).
34. J. K. Karen et al., "Detection of basal cell carcinomas in Mohs excisions with fluorescence confocal mosaicing microscopy," *Br. J. Dermatol.* **160**(6), 1242–1250 (2009).
35. M. J. Smith-Zagone and M. R. Schwartz, "Frozen section of skin specimens," *Arch. Pathol. Lab. Med.* **129**(12), 1536–1543 (2005).
36. L. C. Kelley and L. Starkus, "Immunohistochemical staining of lentigo maligna during Mohs micrographic surgery using MART-1," *J. Am. Acad. Dermatol.* **46**(1), 78–84 (2002).
37. A. D. Stevenson et al., "Systematic review of diagnostic accuracy of reflectance confocal microscopy for melanoma diagnosis in patients with clinically equivocal skin lesions," *Dermatol. Pract. Concept.* **3**(4), 19–27 (2013).
38. S. Debarbieux et al., "Perioperative confocal microscopy of the nail matrix in the management of in situ or minimally invasive subungual melanomas," *Br. J. Dermatol.* **167**(4), 828–836 (2012).
39. E. Cinotti et al., "In vivo and ex vivo confocal microscopy for the management of a melanoma of the eyelid margin," *Dermatol. Surg.* **41**(12), 1437–1440 (2015).
40. S. Debarbieux et al., "Intraoperative diagnosis of nonpigmented nail tumours with ex vivo fluorescence confocal microscopy: 10 cases," *Br. J. Dermatol.* **172**(4), 1037–1044 (2015).
41. A. Leclercq et al., "Ex vivo confocal microscopy: a new diagnostic technique for mucormycosis," *Skin Res. Technol.* **22**(2), 203–207 (2015).
42. B. Dasgeb, T. M. Mohammadi, and D. R. Mehregan, "Use of Ber-EP4 and epithelial specific antigen to differentiate clinical simulators of basal cell carcinoma," *Biomark Cancer* **5**, 7–11 (2013).
43. B. Dasgeb et al., "Multiscale BerEp4 molecular imaging of microtumor phantoms: toward theranostics for basal cell carcinoma," *Mol. Imaging* **13**(6), 7290–2014 (2014).

44. M. Jain et al., "Multiphoton microscopy: a potential intraoperative tool for the detection of carcinoma in situ in human bladder," *Arch. Pathol. Lab. Med.* **139**(6), 796–804 (2015).
45. W. R. Zipfel, R. M. Williams, and W. W. Webb, "Nonlinear magic: multiphoton microscopy in the biosciences," *Nat. Biotechnol.* **21**(11), 1369–1377 (2003).
46. B. Larson et al., "Detection of skin cancer margins in Mohs excisions with high-speed strip mosaicing confocal microscopy: a feasibility study," *Br. J. Dermatol.* **169**(4), 922–926 (2013).
47. E. Cinotti et al., "The 'tissue press': a new device to flatten fresh tissue during ex vivo confocal microscopy examination," *Skin Res. Technol.* **23**(1), 121–124 (2017).
48. D. S. Gareau, "Feasibility of digitally stained multimodal confocal mosaics to simulate histopathology," *J. Biomed. Opt.* **14**(3), 034050 (2009).
49. D. S. Gareau et al., "Rapid screening of cancer margins in tissue with multimodal confocal microscopy," *J. Surg. Res.* **178**(2), 533–538 (2012).
50. E. W. Mu et al., "Use of digitally stained multimodal confocal mosaic images to screen for nonmelanoma skin cancer," *JAMA Dermatol.* **152**(12), 1335–1341 (2016).
51. C. Longo et al., "Ex vivo fluorescence confocal microscopy in conjunction with Mohs micrographic surgery for cutaneous squamous cell carcinoma," *J. Am. Acad. Dermatol.* **73**(2), 321–322 (2015).
52. A. M. Association, "CPT changes 2016: an insider's view," https://www.cms.gov/Medicare/Medicare-Fee-for-Service-Payment/PhysicianFeeSched/PFS-Federal-Regulation-Notices-Items/CMS-1654-F.html.
53. C. Longo et al., "In vivo and ex vivo confocal microscopy for dermatologic and Mohs surgeons," *Dermatol. Clin.* **34**(4), 497–504 (2016).

Manu Jain is an assistant attending and a trained pathologist with expertise in optical imaging (confocal microscopy, multiphoton microscopy, full-field-optical-coherence tomography, etc.), in the Dermatology Department at MSKCC. Currently, she is actively using reflectance confocal microscopy for imaging skin lesions *in vivo* in clinics, as well as fluorescence confocal microscopy in research for the assessment of Mohs surgical margins. She envisions optical imaging as a rapid bedside diagnostic tool for *in vivo* and *ex vivo* imaging.

Milind Rajadhyaksha develops and translates confocal microscopes for noninvasively guiding diagnosis and therapy of skin cancers. His work spans the entire spectrum from laboratory research through commercialization through translational studies to clinical implementation, and he enjoys working in the "valley of death" (and living through near-death experiences). Two of his microscopes have been commercialized (VivaScopes) and are now being used in clinics, with promising early impact on patient care (sparing biopsies of benign lesions).

Kishwer Nehal is a board certified dermatologist with fellowship training/expertise in cutaneous oncology, Mohs and dermatologic surgery at Memorial Sloan-Kettering Cancer Center. She developed and directs the cutaneous oncology, Mohs Surgery, Multidisciplinary Skin Cancer Management Program, and the Micrographic Surgery and Dermatologic Oncology Fellowship. She has published extensively and her clinical research focuses on noninvasive confocal imaging of skin cancers with the optical imaging team at MSKCC, resulting in significant technological advances.